

Affective EEG-Based Person Identification Using the Deep Learning Approach

Theerawit Wilaiprasitporn, Apiwat Ditthapron, Karis Matchaparn, Tanaboon Tongbuasirilai, Nannapas Banluesombatkul and Ekapol Chuangsuanich

Abstract— There are several reports available on affective electroencephalography-based personal identification (affective EEG-based PI), one of which uses a small dataset and another reaching less than 90% of the mean correct recognition rate *CRR*. Thus, the aim of this paper is to improve and evaluate the performance of affective EEG-based PI using a deep learning approach. The state-of-the-art EEG dataset DEAP was used as the standard for affective recognition. Thirty-two healthy participants participated in the experiment. They were asked to watch affective elicited music videos and score subjective ratings for forty video clips during the EEG measurement. An EEG amplifier with thirty-two electrodes was used to record affective EEG measurements from the participants. To identify personal EEG, a cascade of deep learning architectures was proposed, using a combination of Convolutional Neural Networks (CNNs) and Recurrent Neural Networks (RNNs). CNNs are used to handle the spatial information from the EEG while RNNs extract the temporal information. There has been a cascade of CNNs, with recurrent models known as Long Short-Term Memory (CNN-LSTM) and Gate Recurrent Unit (CNN-GRU) for comparison. Experimental results indicate that CNN-GRU and CNN-LSTM can deal with an EEG (4–40 Hz) from different affective states and reach up to 99.90–100% mean *CRR*. On the other hand, a traditional machine learning approach such as a support vector machine (SVM) using power spectral density (PSD) as a feature does not reach 50% mean *CRR*. To reduce the number of EEG electrodes from thirty-two to five for more practical application, F_3 , F_4 , F_z , F_7 and F_8 were found to be the best five electrodes for application in similar scenarios to those in this study. CNN-GRU and CNN-LSTM reached up to 99.17% and 98.23% mean *CRR*, respectively.

In summary, proposed CNN-GRU and CNN-LSTM for EEG-based PI were outperformed the state-of-the art and relevant algorithms (Mahalanobis distance based classifier using PSD/spectral coherence (COH) as features, deep neural network (DNN) and SVM) on the same datasets. In comparison of CNN-GRU and CNN-LSTM, CNN-GRU was obviously better in terms of training speed. Furthermore, mean *CRR* from CNN-GRU was slightly higher than CNN-

This work was supported by The Thailand Research Fund under Grant MRG6180028.

T. Wilaiprasitporn and N. Banluesombatkul are with Bio-inspired Robotics and Neural Engineering Lab, School of Information Science and Technology, Vidyasirimedhi Institute of Science & Engineering, Rayong, Thailand (e-mail: theerawit.w@vistec.ac.th).

A. Ditthapron is with the Computer Department, Worcester Polytechnic Institute, Worcester, MA, USA.

K. Matchaparn is with the Computer Engineering Department, King Mongkut's University of Technology Thonburi, Bangkok, Thailand.

T. Tongbuasirilai is with Department of Science and Technology, Linköping University, Sweden.

E. Chuangsuanich is with the Computer Engineering Department, Chulalongkorn University, Bangkok, Thailand.

LSTM, especially with sparse numbers of electrodes.

Index Terms— Electroencephalography, Personal identification, Biometrics, Deep learning, Affective computing, Convolutional neural networks, Long short-term memory, Recurrent neural networks

I. INTRODUCTION

IN today's world of large and complex data-driven applications, research engineers are inspired to incorporate multiple layers of artificial neural networks or deep learning (DL) techniques into health informatic-related studies in bioinformatics, medical imaging, pervasive sensing, medical informatics and public health [1]. Such studies also include those relating to frontier neural engineering research into brain activity using the non-invasive measurement technique called electroencephalography (EEG). The fundamental concept of EEG involves measuring electrical activity (variation of voltages) across the scalp. The EEG signal is one of the most complex in health data and can benefit from DL techniques in various applications such as insomnia diagnosis, seizure detection, sleep studies, emotion recognition, and Brain-Computer Interface (BCI) [2]–[7]. However, EEG-based Person Identification (PI) research using the DL approach is scarcely found in literature. Thus, we are motivated to work in this direction.

EEG-based PI is a biometric PI system—fingerprints, iris, and face for example. Unlike other biometrics, EEG signals are difficult to collect surreptitiously, since they are concealed within the brain [8]. EEG signals are determined by a person's unique pattern and influenced by stress, and mental state [9], with the potential to protect encrypted data under threat. The PI process shares certain similarities with the person verification process, but their purposes are different. Person verification validates the biometrics to confirm a person's identity (one-to-one matching), while PI uses biometrics to search for an identity match (one-to-many matching) on the database [10]. EEG-based PI system development has dramatically increased in the last century [11], [12]. Eye closing, visual stimulation [13], [14] and multiple mental tasks such as mathematical calculation, writing text, and imagining movements are three major tasks in stimulating brain responses for EEG-based PI [15]. To identify a person, it is very important to investigate the stimulating tasks which can induce personal brain response patterns. Moods, feelings, and attitudes are usually related to personal mental states which react to the

environment. However, to this day, emotion-elicited EEG has not been explored as much as person identification capability. There are several reports on affective EEG-based PI; one with a small dataset [16] and another reaching less than a 90% mean (*CRR*) [17]. Thus, the aim of this paper is to evaluate the usability of EEG from elicited emotions for person identification applications. The study of affective EEG-based PI can help us to gain greater understanding concerning the performance of personal identification among different affective states. Moreover, a developed DL model has been transferred to our ongoing research into personal affective states recognition. This study mainly focuses on a state-of-the-art EEG dataset for emotion analysis named DEAP [18].

A recent critical survey on the usability of EEG-based PI resulted in major signal processing techniques for use in feature extraction and classification [12]. Fourier Methods (PSD) [19]–[22], the Autoregressive Model (AR) [23]–[28], Wavelet Transform (WT) [29], [30] and Hilbert-Huang Transform (HHT) citeKumari2014, Yang2014 are useful for feature extraction. For feature classification, k-Nearest Neighbour (k-NN) algorithms [33], [34], Linear Discriminant Analysis (LDA) [35], [36], Artificial Neural Networks (ANNs) with a single hidden layer [19], [37]–[39] and kernel methods [40], [41] are popular techniques. In this study, a DL technique for both feature extraction and classification is proposed. The proposed DL model is a cascade of the CNN and GRU. CNN and GRU are supposed to capture spatial and temporal information from EEG signals, respectively. A similar cascade model using CNN and LSTM has recently been applied in a motor imagery EEG classification for BCI applications, but GRUs were not studied [5].

The main academic merit of this study concerns affective EEG-based PI using a DL approach, which has not previously been explored to any extent. The study is divided into four experimental parts. The first experiment investigates the performance of different affective EEG states in PI. In the second experiment, the best affective EEG state for PI is used to explore whether or not any EEG frequency bands outperform others for PI purposes. Affective EEG-based PI performance using different sets of sparse EEG electrodes (for practical application purposes) are compared in the third experiment. Finally, in the last experiment, we compare the performance of our proposed cascade model (CNN-GRU) against a conventional spatiotemporal DL model (CNN-LSTM), power spectral density (PSD) features with a support vector machine (SVM), and either PSD or spectral coherence (COH) features with a Mahalanobis distance-based classifier, reproduced from [21]. Moreover, a previous report on EEG-based PI performance from the same datasets using SVM and deep neural network (DNN) is included in the comparison [17]. *CRR* and trainable times (decreasing training loss value by epoch) are used to measure various model configurations of CNN-GRU and CNN-LSTM. The results are promising in that CNN-GRU has a greater decreasing rate of training loss value by epoch than that for CNN-LSTM with a slightly higher mean *CRR*, especially in EEG-based PI using sparse electrodes (five).

The structure of this paper is as follows. Sections II and III present the background and methodology, respectively. The

results are reported in Section IV. Section V discusses the results from two experimental studies. Moreover, the beneficial points are highlighted for comparison over previous works for further investigation. Finally, the conclusion is presented in Section VI.

II. THE DEEP LEARNING APPROACH TO EEG

There has been a surge of deep learning-related methods for classification of EEG signals in recent years. Since EEG signals are recordings of biopotentials across the scalp over time, researchers tend to use DL architectures for capturing both spatial and temporal information. A cascade of CNN, followed by an RNN, often an LSTM, is typically used. These cascade architectures work according to the nature of neural networks, where the proceeding layers function as feature extractors for the latter layers. CNNs, which are good at handling local spatial information, are used initially for learning meaningful patterns. These feature patterns are then used by the LSTM, which can better handle temporal information. Zhang et al. also tried a 3D CNN to exploit the spatiotemporal information directly within a single layer. However, the results were slightly behind a cascade of the CNN-LSTM model [5]. This might be due to the fact that LSTMs are often better at handling temporal information since they can choose to remember and discard information depending on the context.

Another type of recurrent neural network called the Gated Recurrent Unit (GRU) has also been proposed as an alternative to the LSTM [42]. The GRU can be considered as a simplified version of the LSTM. GRUs have two gates (reset and update) instead of three gates as in the LSTMs. GRUs directly output the captured memory, while LSTMs can choose not to output its content due to the output gate. Figure 1 (a) shows the interconnections of a GRU unit. Just as a fully connected layer is composed of multiple neurons, a GRU layer is composed of multiple GRU units. Let \mathbf{x}_t be the input at time step t to a GRU layer. The output of the GRU layer, \mathbf{h}_t , is a vector composing the output of each individual unit h_t^j , where j is the index of the GRU cell. The output activation is a linear interpolation between the activation from the previous time step and a candidate activation, \hat{h}_t^j .

$$h_t^j = (1 - z_t^j)h_{t-1}^j + z_t^j\hat{h}_t^j \quad (1)$$

where an update gate, z_t^j , decides the interpolation weight. The update gate is computed by

$$z_t^j = F^j(W_z \mathbf{x}_t + U_z \mathbf{h}_{t-1}) \quad (2)$$

where W_z and U_z are trainable weight matrices for the update gate, and $F^j()$ takes the j -th index and pass it through a non-linear function (often a sigmoid). The candidate activation is also controlled by an additional reset gate, \mathbf{r}_t , and computed as follows:

$$\hat{h}_t^j = G^j(W \mathbf{x}_t + U(\mathbf{r}_t \odot \mathbf{h}_{t-1})) \quad (3)$$

where \odot represents an element-wise multiplication, and $G^j()$ is often a tanh non-linearity. The reset gate is computed in a

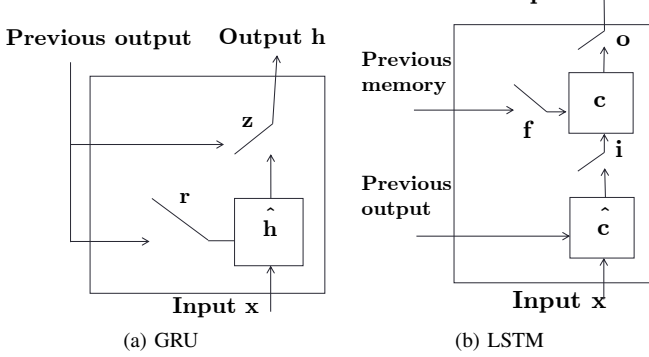


Fig. 1. Comparison between GRU and LSTM structures and their operations

similar manner as the update gate:

$$r_t^j = F^j(W_r \mathbf{x}_t + U_r \mathbf{h}_{t-1}) \quad (4)$$

On the other hand, LSTMs have three gates, input, output, and forget gates which are denoted as i_t^j , o_t^j , f_t^j , respectively. They also have an additional memory component for each LSTM cell, c_t^j . A visualization of an LSTM unit is shown in Figure 1 (b). The gates are calculated in a similar manner as the GRU unit except for the additional term from the memory component.

$$i_t^j = F^j(W_i \mathbf{x}_t + U_i \mathbf{h}_{t-1} + V_i \mathbf{c}_{t-1}) \quad (5)$$

$$o_t^j = F^j(W_o \mathbf{x}_t + U_o \mathbf{h}_{t-1} + V_o \mathbf{c}_t) \quad (6)$$

$$f_t^j = F^j(W_f \mathbf{x}_t + U_f \mathbf{h}_{t-1} + V_f \mathbf{c}_{t-1}) \quad (7)$$

where V_i , V_o , and V_f are trainable diagonal matrices. This keeps the memory components internal within each LSTM unit.

The memory component is updated by forgetting the existing content and adding a new memory component \hat{c}_t^j :

$$c_t^j = f_t^j c_{t-1}^j + i_t^j \hat{c}_t^j \quad (8)$$

where the new memory content can be computed by:

$$\hat{c}_t^j = G^j(W_c \mathbf{x}_t + U_c \mathbf{h}_{t-1}) \quad (9)$$

Note how the updated equation for the memory component is governed by the forget and input gates. Finally, the output of the LSTM unit is computed from the memory modulated by the output gate according to the following equation:

$$h_t^j = o_t^j \tanh(c_t^j) \quad (10)$$

Previous works using deep learning with EEG signals have explored the use of CNN-LSTM cascades [5]. However, GRUs have been shown in many settings to often match or even beat LSTMs [43]–[45]. GRUs have the ability to perform better with a smaller amount of training data and are faster to train than LSTMs. Thus, in this work, CNN-GRU cascades are also explored and compared against the CNN-LSTM in both accuracy and training speed.

TABLE I
AFFECTIVE EEG DATA FORMAT WITH LABEL

Array Name	Array Shape
data	32 x 40 x 32 x 8064 participant x video/trial x EEG x data
labels	32 x 40 x 2 participant x video/trial x (valence, arousal)

III. METHODOLOGY

In this section, we first introduce an affective EEG dataset named DEAP [18], and describe data pre-processing. Due to practicalities, subsampling was carried out from whole datasets for experimental purposes. Finally, the proposed DL approach and its implementation were explained prior to experimentation.

A. Affective EEG Dataset

In this study, we use the state-of-the-art EEG dataset which is standard for emotion or affective recognition, (data_preprocessed_python.zip) [46]. Thirty-two healthy participants participated in the experiment. They were asked to watch affective elicited music videos and score subjective ratings (valence and arousal) for forty video clips during the EEG measurement.

Table I presents a summary of the dataset used. The EEG dataset was pre-processed using the following steps:

- The data was down-sampled to 128 Hz.
- EOG artefacts were removed using the blind source separation technique (independent component analysis or ICA).
- A bandpass frequency filter from 4.0–45.0 Hz was applied to the original datasets. However, the bandpass frequency filters and coined definition of filtered EEG were applied to our experiments as follows: Theta (4–8 Hz), Alpha (8–15 Hz), Beta (15–32 Hz), Gamma (32–40 Hz), and all bands (4–40 Hz).
- The data was averaged to the common reference.
- The EEG channels were reordered so that they all follow the Geneva order as above.
- The data was segmented into 60-second trials and a 3-second pre-trial baseline removed.

Most researchers have been using this dataset to develop an affective computing algorithm; however, we used this affective dataset for studying EEG-based PI.

B. Subsampling and Validation

Affective EEG is categorised by the standard subjective measures of valence and arousal scores (0–9), with 5 as the threshold for defining low (score < 5) and high (score ≥ 5) levels for both valence and arousal. Thus, there were five affective states in total (including all states), as stated in Table II. For practicality, we randomly selected five EEG trials/states (recorded EEG from five video clips) for the experiments. Thus, new users can spend just five minutes watching five videos for the first registration. Table II presents a number of subjects in each affective state. The numbers were different in

TABLE II

NUMBER OF PARTICIPANTS IN EACH STATE OF AFFECTIVE EEG

Affective States	Number of Participants
Low Valence, Low Arousal (LL)	26
Low Valence, High Arousal (LH)	24
High Valence, Low Arousal (HL)	23
High Valence, High Arousal (HH)	32
All States (datasets)	32

each state because some subjects had less than five recorded EEG trials categorised into the state. Furthermore, we aimed to identify a person from a short-length of EEG: 10-seconds. According to Section II A), one EEG trial lasted longer than 60-seconds. Thus, we simply cut one EEG trial into six subsamples. Finally, we had 30 subsamples (6 subsamples \times 5 trials or clips) from each participant in each of the affective states.

In summary, labels in our experiments (personal identification) are ID of participants. Data and labels that have been used can be described as:

- Data: number of participants \times 30 subsamples \times 1280 EEG data points (10-seconds with 128 Hz sampling rate)
- Label: number of participants \times 30 subsamples \times 1(ID)

In all the experiments, the training, validation, and testing sets were obtained using stratified 10-fold cross-validation. Of the subsamples, 80% were used as training, while the validation and test sets each contained 10% of the subsamples.

C. Experiment I: Comparison of affective EEG-based PI among different affective states

Due to the investigated datasets containing EEG from five different affective states (including all states) as shown in Table II, an experiment was carried out to evaluate which affective states would give the highest *CRR* in EEG-based PI applications. To achieve this goal, two approaches were implemented: deep learning and conventional machine learning, for comparison of *CRR* from different affective EEG states. EEG in the range of 4–40 Hz was used in this experiment.

1) *Deep Learning Approach*: Figure 2 demonstrates the preparation of the 10-second EEG data before feeding into the DL model. In general, a single EEG channel is a one-dimensional (1D) time series. However, multiple EEG channels can be mapped into time series of 2D mesh (similar to a 2D image). For each time step, the data point from each EEG channel is combined into one 2D mesh shape of 9×9 . The mean and variance for each mesh (32 channels) is normalised individually. In this study, a non-overlapping sliding window is used to separate the data into one-second chunks. Since the sampling rate of input data is 128 Hz, the window size is 128 points. Thus, for each 10-second EEG data, a $10 \times 9 \times 128$ -dimensional tensor is obtained.

The deep learning model starts with three layers of 2D-CNN (applied to the mesh structure). Each mesh frame from the 128 windows is considered according to its own channel in the 2D-CNN. Since this is also a time series, the 2D-CNN is applied to each sliding window, one window at a time, but with shared parameters. This structure is called a TimeDistributed 2DCNN

layer. After the TimeDistributed 2DCNN layers, a TimeDistributed Fully Connected (FC) layer is used for subsampling and feature transformation. To capture the temporal structure, two recurrent layers (GRU or LSTM) are then applied along the dimension of the sliding windows. Finally, an FC layer is applied to the recurrent output at the final time step with a softmax function for person identification.

The following specific model parameters are used in Experiments I–III. Three layers of TimeDistributed 2DCNNs with kernels measuring 3×3 . The number of filters starts with 128 at the first layer, then 64 and 32, respectively. ReLu nonlinearity is used and batch normalisation and dropout applied after every convolutional layer. For the recurrent layers, we used 2 layers with 32 and 16 recurrent units, respectively. Recurrent dropout was also applied. The dropout rates in each part of the model were fixed at 0.3. We used RMSprop optimizer with a learning rate of 0.003 with a batch size of 256. Although these parameters are held fixed, these settings were found to be good enough to compare the effectiveness between setups for our purposes. The effect of parameter tuning for DL models will be further explored in Experiment IV.

2) *Conventional Machine Learning Approach using Support Vector Machine (SVM)*: The algorithm aims to locate the optimal decision boundaries for maximising the margin between two classes in hyperplane [47]. This can be done using a minimising equation:

$$\frac{1}{2} w^t w + C \sum_{i=1}^n \xi_i, \quad (11)$$

where (11) is under constraint of

$$y_i(w^t \phi(x_i) + b) \geq 1 - \xi_i \text{ and } \xi_i \geq 0, i = 1, \dots, N. \quad (12)$$

C is the capacity constant, w is the vector of coefficients, b is a constant which handles non-separable and data i represents the labels of N training classes. The larger the C value, the more the error is penalised. The C value is optimised to avoid over-fitting, using the validation dataset in this paper.

In the study of person identification, the class label represents the identity number of the participant, considered as a multi-class classification problem. Numerous SVM algorithms can be used such as the "one-against-one" approach, "one-vs-the-rest" approach [47], or k-class SVM [48]. However, since this paper uses SVM to provide the baseline results of traditional machine learning, the "one-against-one" approach is chosen for its robustness towards imbalanced classes and small amounts of data, but it is a computationally expensive classification. The "one-against-one" SVM solves multi-class classification by building classifiers for all possible pairs of classes resulting in $\frac{N(N-1)}{2}$. The predicted class label is the one most yielded from all classifiers.

In this work, Welch's method is employed as the feature extraction method for the SVM. It is a well-known power spectral density estimation method, for reducing variance in the traditional periodogram method by breaking data into overlapped segments. Before feeding into the SVM, a normalisation step is performed. For normalisation, Z-score scaling

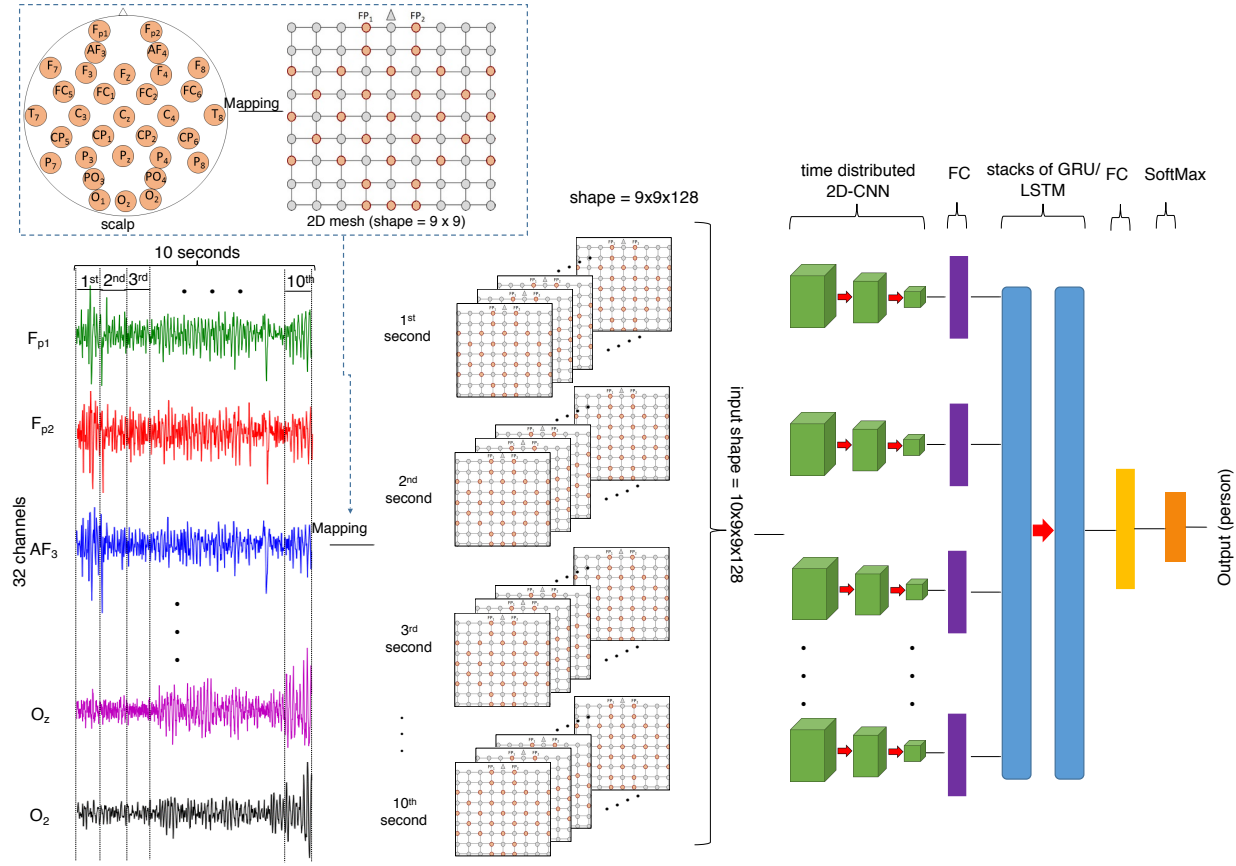


Fig. 2. Implementation of the cascade CNN-GRU/LSTM model according to EEG data. Meshing is the first step in converting multi-channel EEG signals into sequences of 2D images. The 2D mesh time series is passed through the cascade of CNN and recurrent layers for training, validation, and testing.

is adopted, because, experimentally, it performs better than other normalisation methods such as min-max and unity normalisation in EEG signal processing.

$$x_{\text{normalized}} = \frac{x - \bar{x}_{\text{train}}}{s_{\text{train}}} \quad (13)$$

Normalisation parameters, sample mean (\bar{x}_{train}) and sample standard deviation (s_{train}), are computed over the training set, but apply to training, validation, and testing sets separately on each feature. The validation set is used to determine the best parameter C , a penalty parameter of the SVM, from 0.01, 0.1, 1, 10, 100 for each experiment.

Note: according to the results of Experiment I (EX I), all states (whole datasets) of EEG demonstrated the best performance in the DL approach. Thus, this means that affective states do not affect PI performance. Therefore, the affective EEG states were not considered in the remaining experiments.

D. Experiment II: Comparison of affective EEG-based PI among EEGs from different frequency bands

EEG is conventionally used to measure variations in electrical activity across the human scalp. The electrical activity occurs from the oscillation of billions of neural cells inside the human brain. Most researchers define four EEG frequency

bands. Here, we define Theta (4–8 Hz), Alpha (8–15 Hz), Beta (15–32 Hz), Gamma (32–40 Hz) and all bands (4–40 Hz). In this study, we question whether or not frequency bands affect PI performance. To answer the question, we incorporate CNN-LSTM (stratified 10-fold cross-validation), CNN-GRU, and SVM (as performed in EX I) for CRR comparison.

Note: according to the results of Experiment II, all bands (4–40 Hz) provided the best CRR and we continued to use all bands for the remainder of the study.

E. Experiment III: Comparison of affective EEG-based PI among EEGs from sets of sparse EEG electrodes

In this experiment, we questioned whether or not the number of electrodes could be reduced from thirty-two channels to five while maintaining an acceptable CRR. The lower the number of electrodes required, the more user-friendly and practical the system. To investigate the question, we defined sets of five EEG electrodes as shown in Figure 3, including Frontal (F) Figure 3(a), Central and Parietal (CP) Figure 3(b), Temporal (T) Figure 3(c), Occipital and Parietal (OP) Figure 3(d), and Frontal and Parietal (FP) Figure 3(e). According to EX I and II, the DL approach obviously overcomes the traditional SVM in PI applications. Thus, we incorporated only CNN-GRU and CNN-LSTM in this investigation.

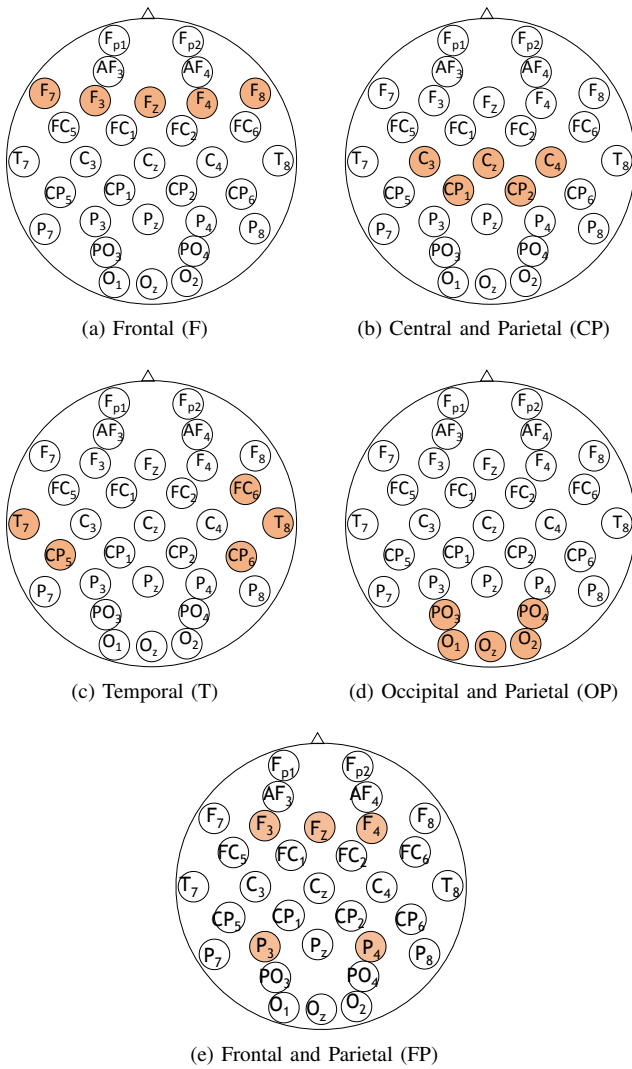


Fig. 3. Experimental Study III evaluates the *CRR* of the EEG-based PI in different sets of sparse EEG electrodes. Five EEG electrode channels from each part of the scalp were grouped into five different configurations (a-e)

In this experiment, we questioned that number of electrode could be reduced from thirty two channels to be five channels while maintaining acceptable *CRR*. The lower number of electrodes are required, the more user friendly and practical of the system is. To investigate the questioning, we defined sets of five EEG electrodes as shown in Figure 3, which included Frontal (F) Figure 3(a), Central and Parietal (CP) Figure 3(b), Temporal (T) Figure 3(c), Occipital and Parietal (OP) Figure 3(d), Frontal and Parietal (FP) Figure 3(e). According to EX I and II, deep learning approach obviously overcomes traditional SVM in PI applications. Thus, we incorporated only CNN-GRU and CNN-LSTM for this investigation.

F. Experiment IV: Comparison of proposed CNN-GRU against CNN-LSTM and other relevant approaches towards affective EEG-based PI application

First, we evaluated our proposed CNN-GRU against a conventional spatiotemporal DL model, namely which CNN-

LSTM [5]. Both approaches have been previously described in detail in Section III and Figure 2. In this study, the parameter settings were varied with a number of CNN layers and GRU/LSTM units for performance evaluation in terms of *CRR* and training speed (decreasing training loss value by epoch) towards the EEG-based PI using thirty-two electrodes. Secondly, the best parameter settings for both CNN-GRU and CNN-LSTM were compared against conventional machine learning and relevant works, such as the Mahalanobis distance-based classifier, using either PSD or spectral coherence (COH) as features (reproduced from [21]) and DNN/SVM on the same datasets as reported in [17].

1) Deep Learning Approach: To find suitable CNN layers for cascading with either GRU or LSTM, the numbers of CNN layers were varied as presented in Table III. The selected CNN layers were then cascaded to GRU/LSTM and the numbers of GRU and LSTM units varied, as can be seen in Table IV.. The dropout rates in each part of the model were fixed at 0.3. We used rmsprop with a learning rate of 0.003 and a batch size of 256. Although these parameters are held fixed, the settings were found to be good enough for the purpose of comparing the effectiveness between setups.

2) Baseline Approach: As previously mentioned, the Mahalanobis distance-based classifier with either PSD or COH as features was used for a baseline comparison of the DL approach and conventional machine learning for EEG-based PI. This approach was reported to provide the highest *CRR* among multiple approaches in a recent critical review paper on EEG-based PI [12]. However, it has never been implemented for DEAP affective datasets as in this study. Thus the previously mentioned approach was reproduced according to the original work [21], applying the DEAP datasets for evaluating *CRR* performance.

To obtain the PSD and COH features, the same parameters were used as reported in [21], except that the number of FFT points was set to 128. Each PSD feature has $N_{PSD} = 32$ elements (electrodes) and each COH feature has $N_{COH} = 496$ elements (pairs). Classification was then performed on the transformed features. Fisher's Z transformation was applied to the COH features and a logarithmic function to the PSD features. After the transformed PSD and COH features for each element were obtained, the Mahalanobis distances, $d_{m,n}$, were then computed as shown in Equation 14.

$$d_{m,n} = (O_m - \mu_n) \Sigma^{-1} (O_m - \mu_n)^T \quad (14)$$

where O_m is the observed feature vector, μ_n is the mean feature vector of class n , and Σ^{-1} is the inverse pooled covariance matrix. The pooled covariance matrix is the averaged-unbiased covariance matrix of all class distributions. For each sample, the Mahalanobis distances were computed between the observed sample m and the class distribution n , thus a distance vector of size N where $N = 32$, representing the number of classes (participants) in the dataset.

The classification methods were proposed with two different schemes. The first scheme was a single-element classification to perform the identification of each electrode separately. The other scheme was the all-element classification, combining all

TABLE III

VARIATION IN THE NUMBER OF CNN LAYERS WITH FIXING GRU/LSTM UNITS

CNN	GRU/LSTM
128	32, 16
128, 64	32, 16
128, 64, 32	32, 16

TABLE IV

VARIATION IN THE NUMBER OF GRU/LSTM UNITS WITH THREE CNN LAYERS IN THIS STUDY

CNN	GRU/LSTM
128, 64, 32	16, 8
128, 64, 32	32, 16
128, 64, 32	64, 32

pairs of electrodes using match score fusion and subsequent identification. Here, we implemented all-element classification. Since [21] proposed the match score fusion algorithm which selected some of the elements for the best *CRR*, the algorithm was modified so that it was comparable to this work. Instead, all elements were used to compute the match scores then classify the new samples by the maximum match scores $S_{m,n}$. The match scores are computed in Equation 15.

$$S_{m,n}^J = \sum_{e=1}^{N_J} \frac{1}{d_{m,n}^e} \quad (15)$$

where $S_{m,n}$ is the match score between the observed sample m and the class distribution n , J is either the PSD or COH feature, N_J is the number of elements which $N_{PSD} = 32$ and $N_{COH} = 496$. Stratified 10-fold cross-validation was also performed on the all-element classification to obtain the mean *CRR*.

IV. RESULTS

Experimental results are reported separately in each study. Then all of them are summarized at the end of the section.

A. Results I: comparison of affective EEG-based PI among different affective states

The comparison of the mean correct recognition rate or *CRR* (with standard error bar) among different affective states and different recognized approaches had been shown in Table V. Statistical testing named one way repeated measures ANOVA (no violation on Sphericity Assumed) with Bonferroni pairwise comparison (post-hoc comparison) had been implemented for comparison of mean *CRR* (stratified 10-fold cross-validation).

In the comparison of *CRR* among different affective states, the statistical results demonstrate that the *EEG (4–40 Hz) from different affective states does not affect the performance of affective EEG-based PI in all recognised approaches* ($F(4)=0.805, p=0.530, F(4)=0.762, p=0.557$ and $F(4)=0.930, p=0.457$ for CNN-GRU, CNN-LSTM, and SVM, respectively).

Moreover, in comparison of *CRR* among different approaches, the statistical results show a significant difference

TABLE V

COMPARISON OF THE MEAN CORRECT RECOGNITION RATE OR *CRR* (WITH STANDARD ERROR BAR) AMONG DIFFERENT AFFECTIVE STATES AND DIFFERENT RECOGNISED APPROACHES. CNN-GRU AND CNN-LSTM SIGNIFICANTLY OUTPERFORMED THE TRADITIONAL SVM IN EVERY AFFECTIVE STATE (INCLUDING ALL STATES), * NOTES $p<0.01$. EEG IN THE RANGE OF 4–40 Hz HAS BEEN USED IN THIS EXPERIMENT.

	CNN-GRU	CNN-LSTM	SVM
LL	99.90 \pm 0.10*	99.79 \pm 0.14*	33.02 \pm 1.58
LH	99.71 \pm 0.19*	100.0*	36.38 \pm 1.71
HL	99.86 \pm 0.14*	99.86 \pm 0.14*	36.25 \pm 2.45
HH	99.87 \pm 0.12*	99.74 \pm 0.26*	33.59 \pm 1.65
All States	100.0*	99.79 \pm 0.14*	33.02 \pm 1.58

in the mean *CRR* among CNN-GRU, CNN-LSTM, and SVM approaches. In pairwise comparison, CNN-GRU and CNN-LSTM significantly outperformed the traditional SVM in every affective state (including all states), $p<0.01$. Both CNN-GRU (in all states) and CNN-LSTM (in LH) reached up to 100% in mean *CRR*. Further reports on comparative studies of CNN-GRU and CNN-LSTM for EEG-based PI against previous works can be seen in Results IV.

B. Results II: comparison of affective EEG-based PI among EEGs from different frequency bands

Here, we report the comparison of the mean correct recognition rate or *CRR* among different EEG frequency bands and different recognized approaches (shown in ??) using the same statistical testing as same as in Section IV A).

In the comparison of *CRR* among different frequency bands, the statistical results demonstrate that *EEG from different frequency bands does not affect the performance of affective EEG-based PI in CNN-GRU and CNN-LSTM approaches* ($F(4)=2.168, p=0.092$ and $F(4)=0.144, p=0.964$ for CNN-GRU and CNN-LSTM, respectively). However, the SVM approach shows that Theta (4–8 Hz) and Alpha (8–15 Hz) provide significantly higher *CRR* than Beta (15–32 Hz), Gamma (32–40 Hz), and all bands (4–40 Hz) ($F(4)=1309.747, p<0.01$ in ANOVA testing and $p<0.01$ in all pairwise comparisons).

Furthermore, in the comparison of *CRR* among different approaches, there were no differences in CNN-GRU, CNN-LSTM, and SVM for low frequency bands (Theta (4–8 Hz) and Alpha (8–15 Hz)). However, CNN-GRU and CNN-LSTM significantly outperformed the SVM in Beta (15–32 Hz), Gamma (32–40 Hz), and all bands (4–40 Hz), $p<0.01$. CNN-GRU and CNN-LSTM reached up to 100% and 99.79%, respectively, in mean *CRR* from stratified 10-fold cross-validation in Gamma and all bands.

C. Results III: Comparison of affective EEG-based PI among EEGs from sets of sparse EEG electrodes

According to Figure 4 (comparison of PI performance among five sets of EEG electrodes (Frontal (F) Figure 3(a), Central and Parietal (CP) Figure 3(b), Temporal (T) Figure 3(c), Occipital and Parietal (OP) Figure 3(d), Frontal and Parietal (FP) Figure 3(e)), one-way repeated measures ANOVA with Bonferroni pairwise comparison (post-hoc) reported that five electrodes in the F set provided a significantly higher mean

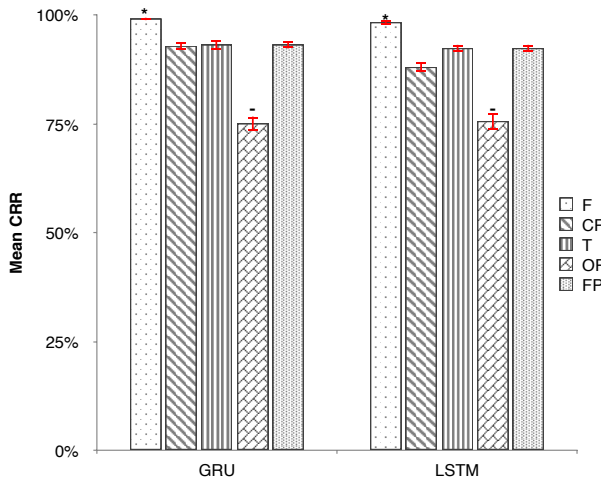


Fig. 4. Comparison of CRR among five sets of electrodes. * Note that the frontal part (F) set provided significantly higher CRR compared to the others $p>0.05$. On the other hand, occipital and parietal (OP) provided significantly lower CRR compared to the others $p<0.05$.

CRR than the other sets in both CNN-GRU $p<0.05$ and CNN-LSTM $p>0.05$. CNN-GRU and CNN-LSTM reached up to $(99.17 \pm 0.34\%)$ and $(98.23 \pm 0.52\%)$ mean CRR, respectively (stratified 10-fold cross-validation). To reduce the number of EEG electrodes from thirty-two to five for more practical application, F_3 , F_4 , F_z , F_7 and F_8 were the best five electrodes for application in similar scenarios to this experiment.

D. Results IV: Comparison of proposed CNN-GRU against CNN-LSTM and the other relevant approaches towards affective EEG-based PI application

Table VI and Table VII present mean CRR (stratified 10-fold cross-validation) from the proposed CNN-GRU against the conventional spatiotemporal DL model, namely CNN-LSTM, in various parameter settings (number of CNN layers and GRU/LSTM units). Mean CRRs from CNN-GRU were higher or equal compared to those from CNN-LSTM in all settings. The standard t-test indicated that the mean CRR CNN-GRU was significantly higher ($p<0.01$) than that of the CNN-LSTM in 3 CNN layers with 128, 64, and 32 filters and 2 layers of GRU/LSTM with 16 and 8 units. In the comparison of training speed between the two approaches, CNN layers were fixed with 128, 64, 32 filters because the mean CRR was equal as shown in Table VI. Figure 5 and Figure 6 present a training speed comparison (in terms of training loss by epoch) from CNN-GRU and CNN-LSTM on 2 layers of GRU/LSTM with 16, 8 and 32, 16 units, respectively. It was obvious that training loss from CNN-GRU was decreasing faster than from CNN-LSTM. These results were also consistent with GRU/LSTM for 64, 32 units.

Table VIII demonstrates EEG-based PI performance using the proposed approach (CNN-GRU) against conventional DL (CNN-LSTM) and the baseline approach, (reproducing Mahalanobis distance-based classifier using PSD/COH as features and DNN and SVM from previous works [17], with the same datasets. CNN-GRU/LSTM (constructed using CNN layers with 128, 64, 32 filters and 2 layers of GRU/LSTM with 32

TABLE VI
COMPARISON OF MEAN CRR RESULTS BETWEEN DIFFERENT CNN LAYERS WITH 32 EEG ELECTRODES

CNN	GRU/LSTM	Mean CRR [%]	
		GRU	LSTM
128	32, 16	100 \pm 0.00	99.69 \pm 0.16
128, 64	32, 16	99.90 \pm 0.10	99.69 \pm 0.16
128, 64, 32	32, 16	99.90 \pm 0.10	99.90 \pm 0.10

TABLE VII
COMPARISON OF MEAN CRR RESULTS BETWEEN DIFFERENT GRU/LSTM UNITS WITH 32 EEG ELECTRODES * NOTE THAT THE MEAN CRR IS SIGNIFICANTLY HIGHER, $p<0.01$.

CNN	GRU/LSTM	Mean CRR [%]	
		GRU	LSTM
128, 64, 32	16, 8	97.29 \pm 0.75 *	89.58 \pm 1.81
128, 64, 32	32, 16	99.90 \pm 0.11	99.90 \pm 0.11
128, 64, 32	64, 32	99.90 \pm 0.11	99.79 \pm 0.25

and 16 units) produced a higher mean CRR than the others. Furthermore, the CNN-GRU was better than CNN-LSTM both in terms of training speed (as shown Figure 5) and mean CRR with a small number of electrodes (five from the frontal area).

V. DISCUSSION

Experimental results towards novelty of this work had been discussed in this section. We mainly discussed two issues, which were physical and algorithmic issue for affective EEG-based PI applications. The physical issue was investigation factors which may affects to PI performance. The factors were different affective states of EEG, frequency bands of EEG and EEG electrode positions on the scalp. The algorithmic issue was about how to implement proposed approach (CNN-GRU) on EEG in the effective way for PI applications and advantages of CNN-GRU over the other relevant approaches.

Regarding the physical issue, the experimental results indicate that DL approaches (CNN-GRU and CNN-LSTM) can deal with EEG (4–40 Hz) from different affective states (valence and arousal levels), reaching up to 100% of mean CRR. On the other hand, a traditional machine learning approach such as SVM using PSD as a feature did not reach 50% of mean CRR. However, the SVM approach was found to improve considerably when focusing on specific EEG frequency bands, namely Theta (4–8 Hz) and Alpha (8–15 Hz). The SVM reached up to 98% of mean CRR with either Theta or Alpha EEG. As to CNN-GRU and CNN-LSTM, EEG frequency bands had no effect, and reached up to 100% and more than 99% of mean CRR, respectively. To reduce the number of EEG electrodes from thirty-two to five for more practical application, F_3 , F_4 , F_z , F_7 and F_8 were the best five electrodes for application in similar scenarios to those in this study. CNN-GRU and CNN-LSTM reached up to 99.17% and 98.23% of mean CRR, respectively. The results show that EEG electrodes from the frontal scalp provided higher mean CRR than other positions on the scalp, which is consistent with previous work on EEG-based PI [21].

Concerning the algorithmic issue, the proposed CNN-GRU and conventional spatiotemporal DL mode (CNN-LSTM) for

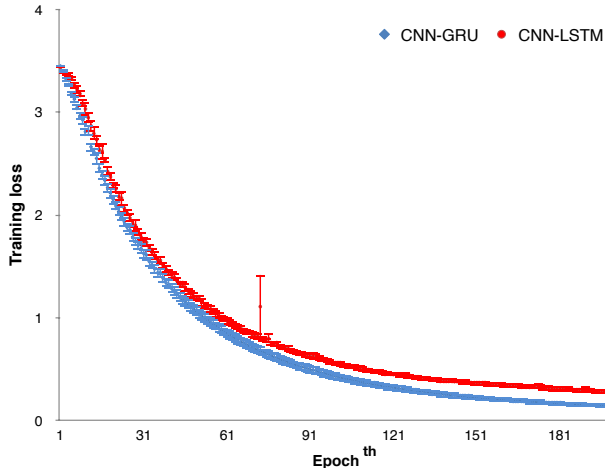


Fig. 5. Comparison of training loss by epoch between CNN-GRU and CNN-LSTM. The configuration consists of 3 CNN layers with 128, 64, 32 filters and 2 layers of GRU/LSTM with 16 and 8 units.

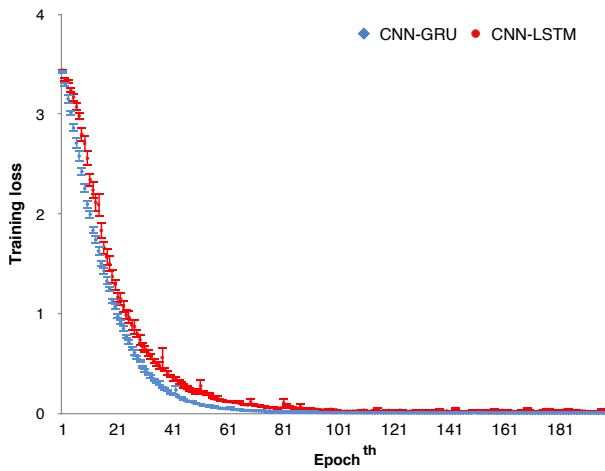


Fig. 6. Comparison of training loss by epoch between CNN-GRU and CNN-LSTM. The configuration consists of 3 CNN layers with 128, 64, 32 filters and 2 layers of GRU/LSTM with 32 and 16 units.

EEG-based PI outperformed the state-of-the-art and relevant algorithms (Mahalanobis distance-based classifier using PSD/COH as features, DNN and SVM [21] [17]) on the same datasets. In the comparison between CNN-GRU and CNN-LSTM, CNN-GRU was obviously better in terms of training speed. Furthermore, the mean *CRR* for CNN-GRU was slightly higher than CNN-LSTM, especially with a sparse number of electrodes.

VI. CONCLUSION

In conclusion, we explored the feasibility of using affective EEG for person identification. We proposed a DL approach called CNN-GRU, as the classification algorithm. EEG-based PI using CNN-GRU reached up to 99.90–100% mean *CRR* with 32 electrodes, and 99.17% with 5 electrodes. CNN-GRU outperformed the state-of-the-art and relevant algorithms (Mahalanobis distance-based classifier using PSD/spectral coherence (COH) as features, DNN and SVM) on the same datasets. In the comparison between CNN-GRU and the conventional

TABLE VIII
COMPARISON OF MEAN *CRR* WITH PROPOSED DL APPROACH (CNN-GRU), CONVENTIONAL DL APPROACH CNN-LSTM, CONVENTIONAL MACHINE LEARNING AND PREVIOUS WORKS ON THE SAME DATASETS.

Approach	Numbers of Electrodes	Mean <i>CRR</i> [%]
CNN-GRU	32	99.90 ± 0.11
CNN-GRU	5	99.10 ± 0.34
CNN-LSTM	32	99.90 ± 0.11
CNN-LSTM	5	98.23 ± 0.52
Mahalanobis-PSD	32	47.09 ± 2.34
Mahalanobis-COH	32	47.81 ± 3.29
DNN [17]	8	85.0 ± 4.0
SVM [17]	8	88.0 ± 4.0

DL cascade model (CNN-LSTM), CNN-GRU was obviously better in terms of training speed. Furthermore, the mean *CRR* from CNN-GRU was slightly higher than from CNN-LSTM, especially with a sparse number of electrodes.

REFERENCES

- [1] D. Ravi, C. Wong, F. Deligianni, M. Berthelot, J. Andreu-Perez, B. Lo, and G.-Z. Yang, "Deep learning for health informatics," *IEEE journal of biomedical and health informatics*, vol. 21, no. 1, pp. 4–21, 2017.
- [2] F. Movahedi, J. L. Coyle, and E. Sejdíć, "Deep belief networks for electroencephalography: A review of recent contributions and future outlooks," *IEEE Journal of Biomedical and Health Informatics*, vol. PP, no. 99, p. 1, 2017.
- [3] M. Shahin, B. Ahmed, S. T. B. Hamida, F. L. Mulaffer, M. Glos, and T. Penzel, "Deep learning and insomnia: Assisting clinicians with their diagnosis," *IEEE Journal of Biomedical and Health Informatics*, vol. 21, no. 6, pp. 1546–1553, Nov. 2017.
- [4] N. Lu, T. Li, X. Ren, and H. Miao, "A deep learning scheme for motor imagery classification based on restricted boltzmann machines," *IEEE Transactions on Neural Systems and Rehabilitation Engineering*, vol. 25, no. 6, pp. 566–576, Jun. 2017.
- [5] D. Zhang, L. Yao, X. Zhang, S. Wang, W. Chen, and R. Boots, "EEG-based intention recognition from spatio-temporal representations via cascade and parallel convolutional recurrent neural networks."
- [6] Y. R. Tabar and U. Halici, "A novel deep learning approach for classification of EEG motor imagery signals," *Journal of neural engineering*, vol. 14, no. 1, p. 016003, 2016.
- [7] R. T. Schirrmeister, J. T. Springenberg, L. D. J. Fiederer, M. Glasstetter, K. Eggensperger, M. Tangermann, F. Hutter, W. Burgard, and T. Ball, "Deep learning with convolutional neural networks for EEG decoding and visualization," *Human brain mapping*, vol. 38, no. 11, pp. 5391–5420, 2017.
- [8] E. Maiorana, D. L. Rocca, and P. Campisi, "On the permanence of eeg signals for biometric recognition," *IEEE Transactions on Information Forensics and Security*, vol. 11, no. 1, pp. 163–175, Jan 2016.
- [9] Q. Gui, Z. Jin, and W. Xu, "Exploring eeg-based biometrics for user identification and authentication," in *2014 IEEE Signal Processing in Medicine and Biology Symposium (SPMB)*, Dec 2014, pp. 1–6.
- [10] J. R. Vacca, *Biometric technologies and verification systems*. Elsevier, 2007.
- [11] P. Campisi and D. L. Rocca, "Brain waves for automatic biometric-based user recognition," *IEEE Transactions on Information Forensics and Security*, vol. 9, no. 5, pp. 782–800, May 2014.
- [12] S. Yang and F. Deravi, "On the usability of electroencephalographic signals for biometric recognition: A survey," *IEEE Transactions on Human-Machine Systems*, vol. 47, no. 6, pp. 958–969, Dec. 2017.
- [13] B. K. Min, H. I. Suk, M. H. Ahn, M. H. Lee, and S. W. Lee, "Individual identification using cognitive electroencephalographic neurodynamics," *IEEE Transactions on Information Forensics and Security*, vol. 12, no. 9, pp. 2159–2167, Sep. 2017.
- [14] Y. Chen, A. D. Atnafu, I. Schlattner, W. T. Weldtsadik, M.-C. Roh, H. J. Kim, S.-W. Lee, B. Blankertz, and S. Fazli, "A high-security EEG-based login system with RSVP stimuli and dry electrodes," *IEEE Transactions on Information Forensics and Security*, vol. 11, no. 12, pp. 2635–2647, 2016.

[15] M. Del Pozo-Banos, J. B. Alonso, J. R. Ticay-Rivas, and C. M. Travieso, "Electroencephalogram subject identification: A review," *Expert Systems with Applications*, vol. 41, no. 15, pp. 6537–6554, 2014.

[16] M. DelPozo-Banos, C. M. Travieso, C. T. Weidemann, and J. B. Alonso, "EEG biometric identification: a thorough exploration of the time-frequency domain," *Journal of neural engineering*, vol. 12, no. 5, p. 056019, 2015.

[17] L. Y., Z. Y., T. T., L. N., and F. Y., "Personal identification based on content-independent eeg signal analysis," *Lecture Notes in Computer Science*, vol. 19568, 2017.

[18] S. Koelstra, C. Muhl, M. Soleymani, J. S. Lee, A. Yazdani, T. Ebrahimi, T. Pun, A. Nijholt, and I. Patras, "DEAP: A database for emotion analysis using physiological signals," *IEEE Transactions on Affective Computing*, vol. 3, no. 1, pp. 18–31, Jan. 2012.

[19] M. Poulos, M. Rangoussi, and N. Alexandris, "Neural network based person identification using EEG features," in *Acoustics, Speech, and Signal Processing, 1999. Proceedings., 1999 IEEE International Conference on*, vol. 2. IEEE, 1999, pp. 1117–1120.

[20] R. Palaniappan and D. P. Mandic, "Biometrics from brain electrical activity: A machine learning approach," *IEEE transactions on pattern analysis and machine intelligence*, vol. 29, no. 4, pp. 738–742, 2007.

[21] D. La Rocca, P. Campisi, B. Vegso, P. Cserti, G. Kozmann, F. Babiloni, and F. D. V. Fallani, "Human brain distinctiveness based on EEG spectral coherence connectivity," *IEEE Transactions on Biomedical Engineering*, vol. 61, no. 9, pp. 2406–2412, 2014.

[22] G. Safont, A. Salazar, A. Soriano, and L. Vergara, "Combination of multiple detectors for EEG based biometric identification/authentication," in *Security Technology (ICCST), 2012 IEEE International Carnahan Conference on*. IEEE, 2012, pp. 230–236.

[23] M. Poulos, M. Rangoussi, V. Chrissikopoulos, and A. Evangelou, "Parametric person identification from the EEG using computational geometry," in *Electronics, Circuits and Systems, 1999. Proceedings of ICECS'99. The 6th IEEE International Conference on*, vol. 2. IEEE, 1999, pp. 1005–1008.

[24] R. Paranjape, J. Mahovsky, L. Benedicenti, and Z. Koles, "The electroencephalogram as a biometric," in *Electrical and Computer Engineering, 2001. Canadian Conference on*, vol. 2. IEEE, 2001, pp. 1363–1366.

[25] A. Riera, A. Soria-Frisch, M. Caparrini, C. Grau, and G. Ruffini, "Unobtrusive biometric system based on electroencephalogram analysis," *EURASIP Journal on Advances in Signal Processing*, vol. 2008, p. 18, 2008.

[26] P. Campisi, G. Scarano, F. Babiloni, F. D. Fallani, S. Colonnese, E. Maiorana, and L. Forastiere, "Brain waves based user recognition using the "eyes closed resting conditions" protocol," in *Information Forensics and Security (WIFS), 2011 IEEE International Workshop on*. IEEE, 2011, pp. 1–6.

[27] E. Maiorana, J. Solé-Casals, and P. Campisi, "EEG signal preprocessing for biometric recognition," *Machine Vision and Applications*, vol. 27, no. 8, pp. 1351–1360, 2016.

[28] Z. Dan, Z. Xifeng, and G. Qiangang, "An identification system based on portable EEG acquisition equipment," in *Intelligent System Design and Engineering Applications (ISDEA), 2013 Third International Conference on*. IEEE, 2013, pp. 281–284.

[29] C. N. Gupta, Y. U. Khan, R. Palaniappan, and F. Sepulveda, "Wavelet framework for improved target detection in oddball paradigms using P300 and gamma band analysis," *Biomedical Soft Computing and Human Sciences*, vol. 14, no. 2, pp. 61–67, 2009.

[30] S. Yang and F. Deravi, "Wavelet-based EEG preprocessing for biometric applications," in *Emerging Security Technologies (EST), 2013 Fourth International Conference on*. IEEE, 2013, pp. 43–46.

[31] P. Kumari, S. Kumar, and A. Vaish, "Feature extraction using empirical mode decomposition for biometric system," in *Signal Propagation and Computer Technology (ICSPCT), 2014 International Conference on*. IEEE, 2014, pp. 283–287.

[32] S. Yang and F. Deravi, "Novel HHT-based features for biometric identification using EEG signals," in *Pattern Recognition (ICPR), 2014 22nd International Conference on*. IEEE, 2014, pp. 1922–1927.

[33] A. Yazdani, A. Roodaki, S. Rezatofighi, K. Misaghian, and S. K. Setarehdan, "Fisher linear discriminant based person identification using visual evoked potentials," in *Signal Processing, 2008. ICSP 2008. 9th International Conference on*. IEEE, 2008, pp. 1677–1680.

[34] F. Su, L. Xia, A. Cai, and J. Ma, "Evaluation of recording factors in EEG-based personal identification: A vital step in real implementations," in *Systems Man and Cybernetics (SMC), 2010 IEEE International Conference on*. IEEE, 2010, pp. 3861–3866.

[35] R. Palaniappan, "Electroencephalogram signals from imagined activities: A novel biometric identifier for a small population," in *International Conference on Intelligent Data Engineering and Automated Learning*. Springer, 2006, pp. 604–611.

[36] H. J. Lee, H. S. Kim, and K. S. Park, "A study on the reproducibility of biometric authentication based on electroencephalogram (EEG)," in *Neural Engineering (NER), 2013 6th International IEEE/EMBS Conference on*. IEEE, 2013, pp. 13–16.

[37] R. Palaniappan, "Method of identifying individuals using VEP signals and neural network," *IEE Proceedings-Science, Measurement and Technology*, vol. 151, no. 1, pp. 16–20, 2004.

[38] R. Palaniappan, J. Gosalia, K. Revett, and A. Samraj, "Pin generation using single channel EEG biometric," *Advances in Computing and Communications*, pp. 378–385, 2011.

[39] Q. Gui, Z. Jin, and W. Xu, "Exploring EEG-based biometrics for user identification and authentication," in *Signal Processing in Medicine and Biology Symposium (SPMB), 2014 IEEE*. IEEE, 2014, pp. 1–6.

[40] H. Jian-feng, "Comparison of different classifiers for biometric system based on EEG signals," in *Information Technology and Computer Science (ITCS), 2010 Second International Conference on*. IEEE, 2010, pp. 288–291.

[41] C. Ashby, A. Bhatia, F. Tenore, and J. Vogelstein, "Low-cost electroencephalogram (EEG) based authentication," in *Neural Engineering (NER), 2011 5th International IEEE/EMBS Conference on*. IEEE, 2011, pp. 442–445.

[42] K. Cho, B. van Merriënboer, D. Bahdanau, and Y. Bengio, "On the properties of neural machine translation: Encoder-decoder approaches."

[43] J. Chung, C. Gulcehre, K. Cho, and Y. Bengio, "Empirical evaluation of gated recurrent neural networks on sequence modeling."

[44] Z. Tang, Y. Shi, D. Wang, Y. Feng, and S. Zhang, "Memory visualization for gated recurrent neural networks in speech recognition."

[45] H.-G. Kim and J. Y. Kim, "Acoustic event detection in multichannel audio using gated recurrent neural networks with high-resolution spectral features," *ETRI Journal*, vol. 39, no. 6, pp. 832–840, 2017.

[46] [Online]. Available: <http://www.eecs.qmul.ac.uk/mmv/datasets/deap/readme.html>

[47] J. Weston and C. Watkins, "Multi-class support vector machines," Citeseer, Tech. Rep., 1998.

[48] S. Knerr, L. Personnaz, and G. Dreyfus, "Single-layer learning revisited: a stepwise procedure for building and training a neural network," in *Neurocomputing*. Springer, 1990, pp. 41–50.